Available online at www.sciencedirect.com

ScienceDirect

Advances in Space Research 62 (2018) 2977–2987

Vol. 62, No. 11, December 2018
doi: 10.1016/j.asr.2018.07.021

ADVANCES IN SPACE RESEARCH (a COSPAR publication)

www.elsevier.com/locate/asr

Contactless electrostatic detumbling of axi-symmetric GEO objects with nominal pushing or pulling

Trevor Bennett *[,1], Hanspeter Schaub [2]

University of Colorado Boulder, Aerospace Engineering Sciences, 431 UCB, Colorado Center for Astrodynamics Research, Boulder, CO 80309-0431, United States

Received 1 March 2017; received in revised form 6 July 2018; accepted 20 July 2018
Available online 15 September 2018

Abstract

Large asset values of satellites and demand for orbital slots in the Geostationary orbit belt motivates on-orbit servicing and active debris removal strategies. The challenge of on-orbit capture of tumbling serviceable satellites or debris targets is primarily overcome by including a target detumble prior to any mechanical interface. Of the many methods proposed, touchless electrostatic detumbling shows significant advantages in collision avoidance and preservation of the target object. Previous studies demonstrated that the electrostatic interaction is sufficient to touchlessly despin the fixed-axis rotation of a rocket body-sized object within several days. This work focuses on large, generally tumbling axi-symmetric targets in the Geostationary Orbit which form a large component of the GEO debris population. The deep-space controller is augmented for tugging, pushing, and nominal detumbling configurations, providing a complete analysis of the stability and convergence properties. The effectiveness of this detumble control is numerically illustrated by simultaneously detumbling and tugging the target in GEO. The controller reduces the tumbling to the order of the mean motion allowing for mechanical docking methods.

Keywords: Touchless detumble; On-orbit debris; Contactless servicing

1. Introduction

The large asset values of Geostationary orbit (GEO) satellites and the significant demand for orbit slots are prime motivations for developing on-orbit servicing and active debris removal (ADR) strategies. In a recent report, the collection of GEO satellites was insured for over 13 Billion US dollars (Chrystal et al., 2011). Protection of these assets and the delivery of newer satellites require that satellite operators adhere to the strict end-of-life practice of boosting these satellites to a higher graveyard orbit to vacate the orbital slot. These practices ensure that uncontrolled satellites and objects are relocated; forestalling a disintegration of currently viable orbits (Anderson and Schaub, 2015). In addition, removing a few key debris objects could drastically reduce the collision risks, reduce fuel expenditure for collision avoidance, and extend the operational life for satellites in the prized Geostationary (GEO) belt (Anderson and Schaub, 2015). The GEO orbit belt is a prime candidate for improved satellite servicing and removal strategies.

Satellite servicing and debris removal are both challenging space mission concepts that require an active command vehicle to approach and mechanically interface with a defunct satellite or satellite component (Couzin et al., 2013; Ogilvie et al., 2008; Xu et al., 2011). Significant attention to this problem is marked by technical advances in

* Corresponding author.
E-mail address: Trevor.Bennett@Colorado.edu (T. Bennett).
[1] Graduate Research Assistant.
[2] Alfred T. and Betty E. Look Professor of Engineering, Associate Chair of Graduate Affairs.

https://doi.org/10.1016/j.asr.2018.07.021
0273-1177/

robotic manipulator capture, soft-docking, flexible structure tethering, and in touchless actuation techniques. Robotic manipulator capture, or conventional capture with the servicer circumnavigating a tumbling target, are limited by a 1 degree per second target tumble rate by control rate and fuel usage (Couzin et al., 2012). Target tumble rates have been observed and modeled for tumble rates up to 10's of degrees per second requiring that the first phase of a servicer mission integrate a strategy for detumbling the target object (Karavaev et al., 2004; Albuja et al., 2015). There are a variety of proposed flexible interface or touchless methods that are not constrained by the target object tumble rate. Notably, deployable net capture and harpoon attachments are among proposed methods (Reed et al., 2012; Starke et al., 2009). While the capture technique overcomes the limitations on target tumble rates, the tethered system requires complicated dynamical modeling and control approaches (Jasper and Schaub, 2014). In an attempt to make the detumble semi-touchless, Reference Caubet and Biggs (2014) proposes a harpoon attached magnetic detumbling device. The attitude stabilization electromagnetic module (ASEM) would interact with Earth's magnetic field to detumble large objects with an example of a 6-ton satellite arrested from 6°/sec tumble in 21 days. Alternatively, a servicer generating eddy-currents in the target craft can capitalize on Earth's magnetic field for complete detumble (Praly et al., 2012; Gómez and Walker, 2015, 2016).

A Line-of-sight proposed mission concept that touchlessly actuates on a debris object is the Ion Beam Shepherd method (Bombardelli and Pelaez, 2011;Kitamura et al., 2012; Bombardelli et al., 2011). Predominantly used to change the orbit of the debris object, the focused exhaust cone of an ion engine may also be directed at particular facets of the target to generate desired torques. While this approach benefits as a touchless method, imprecise knowledge of the thrust plume or time-varying target orientation can cause strong departure motions. Similar to Ion Beam Shepherd, laser ablation of the target is a line-of-sight detumble method that ablates the target object such that the ejected thrust plume provides the desired detumbling torque (Vatrisano et al., 2015, 2016). However, both Ion Beam Shepherd and laser ablation can damage the serviceable object by the impingement of a charged plume and the ablation of the target respectively. Electrostatic detumble addresses the present need of touchlessly detumbling target objects without the negative outcomes of thrust plumes or ablation. The electrostatic detumble mission concept, as shown in Fig. 1, requires a servicing craft to modulate charge transfer via an electron or ion gun such that a differential electrostatic detumble torque is generated.

Electrostatic actuation of spacecraft finds roots in the 1960s with continued research into understanding charging dynamics and development of electrostatic control applications for Earth-orbiting satellites (King et al., 2002). Specifically, the GEO orbit environment is a prime candidate region where space plasma conditions enable electrostatic interaction across 10's to 100's of meters requiring only Watt-levels of power (Cover et al., 1966). Satellites in GEO must account for these effects while researchers have sought to capitalize with the example developments of formation flying concepts and inflatable structures (Berryman and Schaub, 2007; Seubert et al., 2012; Stiles et al., 2013; Wang and Schaub, 2011; Peck et al., 2005; Streetman and Peck, 2007). The concept of electrostatic actuation has extended even to touchless asteroid spin control (Murdoch et al., 2008a,b). Earlier work explores charged formation flying with Coulomb debris tug trajectories (Hogan and Schaub, 2012, 2013) and use Coulomb and Lorentz forces. This suggests that electrostatic actuation is also viable for servicer-driven orbital maneuvering (Yamamoto and Yamakawa, 2008;Peck et al., 2007; Yamakawa et al., 2010). Reference Schaub and Stevenson (2012) discusses the concept in Fig. 1 where electrostatic force fields can be controlled to apply torques on a single-axis-spinning debris object without requiring physical contact. The target object charging is controlled through servicer-emitted electrons or ions which charges the servicer and the target to desired electrostatic potentials. The resulting modulated potential difference creates the attractive force capable of detumbling the target object.

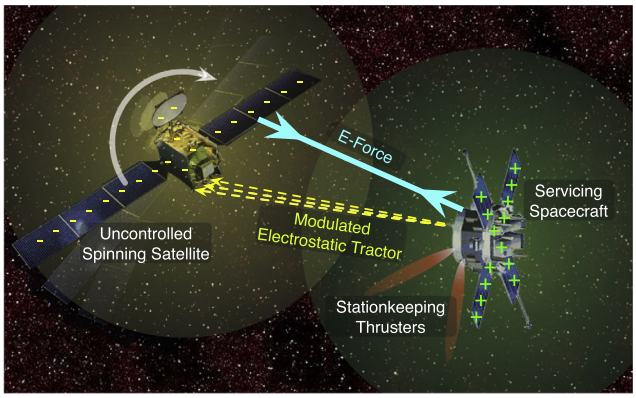

Fig. 1. Electrostatic actuation technology enabling diverse service mission profiles.

The extension of the despin concept led to the recently developed deep space 3-dimensional detumble controller in Reference Bennett and Schaub (2015) which provides analytical predictions of the steady-state cylinder attitude and residual momentum. The deep space controller, which neglects the relative position change due to orbital motion, is viable for the primary on-orbit detumble of a target where the tumble rate of the target is much greater than that of the orbital motion (Bennett and Schaub, 2015). Assuming the relative attitude is dominated by the tumbling of the target simplifies the governing equations. Furthermore, the change in relative attitude due to orbital motion at GEO is on the order of the mean motion which is often in the noise of an attitude sensor-filter system. The

sensitivity to relative motion is explored by applying the deep space controller to on-orbit GEO detumble (Bennett and Schaub, 2016). The resulting numerical optimization analysis demonstrates that the deep space controller is viable on-orbit and also particular relative orbits enhance the detumble relative geometry and reduce the detumble time. Particularly, the lead-follower servicer-target formation is one of several key detumble formations to achieve minimal detumble time (Bennett and Schaub, 2016). The benefits of on-orbit motion are graphically represented by the change in detumble geometry shown in Fig. 2.

As part of GEO servicing missions, it is often required or advantageous to perform a re/de-orbit maneuver either to re-insert the serviced satellite or to remove the debris to a graveyard orbit. Earlier work shows that an electrostatic servicer spacecraft could successfully provide orbit corrections or re-orbit target objects (Hogan and Schaub, 2012, 2013). However, electrostatic tugging and pushing has been demonstrated in the absence of any detumble control. Therefore, it is of great interest to develop and study an electrostatic servicer control that is capable of simultaneous detumbling and tugging/pushing actuation of the target. The deep space controller in Reference Bennett and Schaub (2016) demonstrates that a controller formulated for deep space applications is viable for GEO detumble and is a prime candidate approach to be augmented with tugging/pushing capability.

Addressed by this work are the current challenges of including tug and push capability for orbital maneuvering and to determine stability of the augmented controller for on-orbit applications. This work focuses on large, cylindrical upper stage rocket bodies which form a large component of the GEO debris population. Review of the electrostatic Multi-Sphere method modeling technique and deep space control developments are presented. The deep space controller is augmented with a nominal tugging or pushing term to investigate the resulting stability properties. The work concludes with three on-orbit numerical simulations of electrostatic detumble.

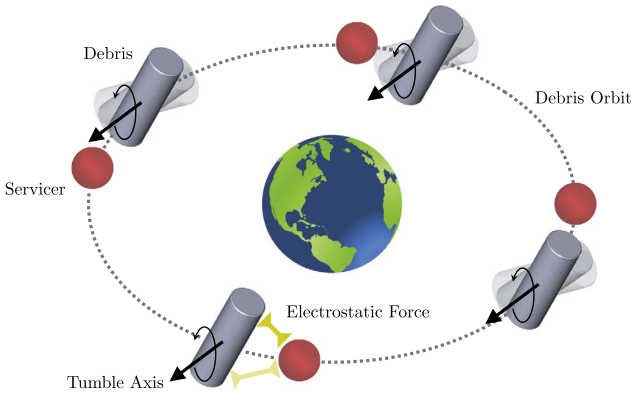

Fig. 2. Representative relative motion of servicer spacecraft around tumbling debris object.

2. Electrostatic modeling

The electrostatic interaction between two craft is accurately approximated for faster than real time control and simulation applications by the Multi-Sphere Method (MSM). MSM represents the spacecraft electrostatic charging model as a collection of spherical conductors carefully dispersed through the body (Stevenson and Schaub, 2013). This method allows for time-varying charge distributions across the spacecraft by coupling the instantaneous relative attitude and the position of body-fixed sphere distributions. Consider a cylindrical target object representative of a depleted upper-stage booster, a dual-spin spacecraft, or a variety of other spacecraft. The cylinder object is electrostatically manipulated by the collection of electrostatic forces induced by the presence of a charged spherical servicer spacecraft as shown in Fig. 3. The 3-sphere MSM cylinder configuration used in this study is generated by matching the force, torque, and capacitance outputs of the commercial software package Maxwell for a variety of attitudes and ranges (Stevenson and Schaub, 2013). The validated MSM model is used in faster-than-real-time simulations and control developments because the otherwise large number of finite elements required to compute charge distribution has been reduced to a small number of body-fixed spheres. The time-varying charges are computed from the prescribed electric potentials according to the self and mutual capacitance relationships in (1) where ϕ is the potential relative to the ambient plasma ground, $k_c = 8.99 \times 10^9$ N·m^2/C^2, and q_i is the charge of each sphere (Smythe, 1968; Sliško and Brito-Orta, 1998).

$$\phi_i = k_c \frac{q_i}{R_i} + \sum_{j=1, j\neq i}^{m} k_c \frac{q_j}{r_{i,j}} \tag{1}$$

The term R_i denotes the radius of the i^{th} conducting sphere and $r_{i,j}$ denotes the vector between the i^{th} and j^{th} conducting spheres. These relations can be collected in matrix form where a, b, c are the centers of the cylinder spheres relative to servicer sphere. Spacecraft that are largely conducting or are shrouded in a conducting layer can be assumed to hold an isopotential. This electrostatic potential constraint is enforced in (2) by using the same potential for all the spheres on the second body, ϕ_2

$$\begin{bmatrix} \phi_1 \\ \phi_2 \\ \vdots \\ \phi_2 \end{bmatrix} = k_c \underbrace{\begin{bmatrix} 1/R_1 & 1/r_a & 1/r_b & 1/r_c \\ 1/r_a & 1/R_{2,a} & 1/l & 1/2l \\ 1/r_b & 1/l & 1/R_{2,b} & 1/l \\ 1/r_c & 1/2l & 1/l & 1/R_{2,c} \end{bmatrix}}_{\text{Elastance}} \begin{bmatrix} q_1 \\ q_a \\ q_b \\ q_c \end{bmatrix} \tag{2}$$

Inverting the Elastance matrix and right-multiplying the spacecraft potentials at a given instant in time and right-multiplying by the potential vector produces the instantaneous charge on each sphere. The sphere-to-sphere electrostatic forces are computed using the charges residing on each sphere shown in Fig. 3. The forces and torques on

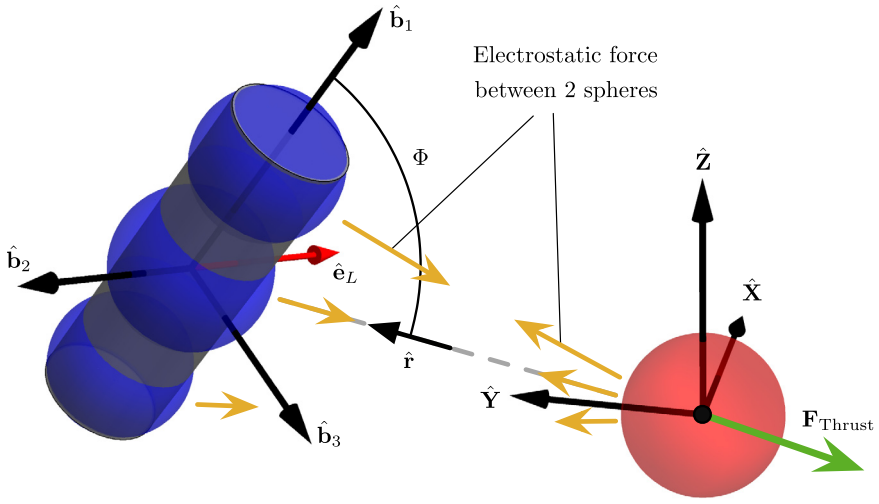

Fig. 3. 3 sphere MSM cylinder and spherical spacecraft configuration.

the cylinder are given by the summation of all sphere-to-sphere forces between the servicer and the target in (3a). Similarly, the torques in (3b) are computed given the relative attitude between the two crafts. Subscripts 1 and 2 refer to respectively the servicer and the target.

$$\boldsymbol{F}_2 = k_c q_1 \sum_{i=a}^{c} \frac{q_i}{r_i^3} \boldsymbol{r}_i \tag{3a}$$

$$\boldsymbol{L}_2 = k_c q_1 \sum_{i=a}^{c} \frac{q_i}{r_i^3} \boldsymbol{r}_{2,i} \times \boldsymbol{r}_i \tag{3b}$$

As seen in Eq. (2), the growth of the square matrix as model fidelity increases and the position-dependent coupling between the potential and charge inhibit obtaining analytical insight in electrostatic detumble behavior for complex systems. An analytic approximation of the MSM torque is utilized so that the control developments, the equilibrium states, and the stability of the system are more easily explored (Schaub and Stevenson, 2012).

3. Deep space detumble with nominal tugging and pushing

The following section develops the deep space detumble attitude dynamics and stability arguments when a nominal attractive or repulsive potential is prescribed. The nominal potential serves as a tug or push to translate the entire system with the separation distance controlled by conventional servicer thrusting. Investigating the deep space scenario first provides two distinct benefits. First, operational electrostatic detumbling requires the space objects to be flying only multiple craft radii apart. Differential gravity will have a small impact on the relative orbit and is absent in the deep space case. Further, the deep space scenario only requires knowledge of the relative orientation of the debris with respect to the servicer while maintaining a fixed relative position of the servicer allows for simplified servicer thrusting implementations. The following analysis considers a deep space scenario to gain analytical insight into the stability and convergence of this detumble control.

3.1. Debris attitude description

The detumble control, developed previously (Bennett et al., 2015) without considering tugging or pushing, relies on the simplified dynamics achieved for the given spherical servicer craft and cylindrical debris object. The axisymmetric debris object with internal MSM spheres does not have a torque component about the cylinder slender axis, the $\hat{\boldsymbol{b}}_1$ axis (Bennett et al., 2015). The torque axis and projection angle Φ about the torque axis defined in Fig. 3 are computed with Eqs. (4) and (5) respectively.

$$\hat{\boldsymbol{e}}_L = \hat{\boldsymbol{b}}_1 \times (-\hat{\boldsymbol{r}}) \tag{4}$$

$$\Phi = \arccos\left(\hat{\boldsymbol{b}}_1 \cdot (-\hat{\boldsymbol{r}})\right) \tag{5}$$

where $\hat{\boldsymbol{r}}$ is the unit direction from the servicer spacecraft mass center to the tumbling body mass center, or the direction of the relative position vector. It was shown in Reference Bennett et al. (2015) that, through the use of this projection angle of a cylinder slender axis onto the relative position vector, the coupled three dimensional rotation equations of motion reduce to scalar equations of the form in Eq. (6). Consistent with the assumption of an axisymmetric geometry, there exists no control authority in the slender axis scalar equation because no cross coupling is present. The presented form is accurate for an inertially fixed relative position vector.

$$I_a \dot{\omega}_1 = 0 \tag{6a}$$

$$I_t \dot{\eta} - I_a \omega_1 \dot{\Phi} \sin\Phi = 0 \tag{6b}$$

$$I_t \left(\ddot{\Phi} \sin\Phi - \eta^2 \frac{\cos\Phi}{\sin^2\Phi} \right) + I_a \omega_1 \eta = L \tag{6c}$$

where I_a is the axial moment of inertia, I_t is the transverse moment of inertia, and the pseudo angular velocities are

defined by components of the body angular velocities ω_i and

$$\eta \equiv -\omega_2\left(\hat{\boldsymbol{r}}\cdot\hat{\boldsymbol{b}}_2\right)-\omega_3\left(\hat{\boldsymbol{r}}\cdot\hat{\boldsymbol{b}}_3\right) \tag{7a}$$

$$\dot{\Phi}\sin\Phi = -\omega_2\left(\hat{\boldsymbol{r}}\cdot\hat{\boldsymbol{b}}_3\right)+\omega_3\left(\hat{\boldsymbol{r}}\cdot\hat{\boldsymbol{b}}_2\right) \tag{7b}$$

$$\boldsymbol{L} = -L\hat{\boldsymbol{e}}_L = -f(\phi)\sin(2\Phi)\hat{\boldsymbol{e}}_L \tag{7c}$$

The following is a control law that successfully drives the projection angle rate to zero. Without loss of generality, the non-cooperative cylinder is assumed to have the same potential magnitude as the servicer, that is $\phi_2 = |\phi_1|$, and is assumed to be always positive (Schaub and Stevenson, 2012). Thus, the voltage dependency function which defines the commanded servicer spacecraft potential is set to Schaub and Stevenson (2012):

$$f(\phi) = \phi|\phi| \tag{8}$$

This assumption is consistent with the control stability analysis first proposed by Reference Schaub and Stevenson (2012) and further developed in Reference Bennett et al. (2015):

$$f(\phi_1) = -\mathrm{sgn}\left(\sum_{m=1}^{n} g_m(\Phi)\right) f(\phi_{\max})\frac{\arctan\left(\alpha\dot{\Phi}\right)}{\pi/2} \tag{9}$$

where $\alpha > 0$ is a constant feedback gain and $f(\phi_{\max})$ is the maximum feasible potential available. The control law as shown in Eq. (12) provides proven asymptotic reduction of the projection angle rate (Bennett et al., 2015). However, the previously developed form does not provide nominal pushing or pulling control authority nor a stability proof for such cases. The following section details the inclusion of nominal pushing and pulling into the control formulation and provides a Lyapunov proof of stability of the expanded form.

3.2. Detumble control with nominal tugging and pushing

In addition to the nominal detumble control, it is desired that the control could also detumble the target while the servicing spacecraft is imparting a nominal push or pull on the debris object. The electrostatic push or pull is obtained by a non-zero nominal control potential with discussion constrained to an inertially fixed relative position vector actively maintained by the servicer. Consider a proposed Lyapunov function of the form

$$V\left(\Phi,\dot{\Phi}\right) = \frac{1}{2}\boldsymbol{\omega}^T I\boldsymbol{\omega} + \beta\int_0^{\Phi} g_m(x)\mathrm{d}x \tag{10}$$

where $g_m(x)$ is specifically for this application

$$g_m(\Phi) = \sum_{m=1}^{n}\gamma_m\sin(2\Phi) \tag{11}$$

The number of basis function terms n are matched with weighting coefficients γ_m (Bennett et al., 2015). A value of $n = 1$ and $gamma_1 = 1$ is sufficient for the larger separation distances considered in this study. The Lyapunov function substitutes a more general projection angle Φ and more general $g_m(\Phi)$ into a Lyapunov function proposed in Reference Schaub and Stevenson (2012). A distinct advantage of the projection angle is that it follows the same form as a 1-dimensional rotation and can therefore encapsulate and utilize previous 1-dimensional control insights. Revising the control formulation for 3-dimensional rotations leads to the new control law for controlling the servicer electrostatic potential $f(\phi_1)$:

$$f(\phi_1) = -\mathrm{sgn}\left(\sum_{m=1}^{n} g_m(\Phi)\right) h\left(\alpha\dot{\Phi}\right) \tag{12}$$

where $\alpha > 0$ is a constant feedback gain and the function h is chosen for stability so that Schaub and Stevenson (2012):

$$h(x)x > 0 \quad \text{if } x \neq 0 \tag{13}$$

For this study, the following function h is proposed:

$$h\left(\alpha\dot{\Phi}\right) = f(\phi_{\max})\frac{\arctan\left(\alpha\dot{\Phi}\right)}{\pi/2} \tag{14}$$

The Lyapunov function in Eq. (10) is positive definite when the monotonically decreasing magnitude restriction $\gamma_m > \gamma_{m+1}$ is placed on γ_m for the projection angle function $g(x)$ (Bennett et al., 2015).

The assurance of a positive definite Lyapunov function enables the time derivative of Eq. (10) to be taken for Lyapunov stability analysis:

$$\dot{V}\left(\Phi,\dot{\Phi}\right) = \boldsymbol{\omega}^T\boldsymbol{L} + \beta g_m(\Phi)\dot{\Phi} \tag{15}$$

Including the detumbling control torque into the Lyapunov derivative and collecting terms, the simplified form of Eq. (15) becomes Eq. (16).

$$\dot{V}\left(\Phi,\dot{\Phi}\right) = [f(\phi_1)\sin\Phi + \beta]g_m(\Phi)\dot{\Phi} \tag{16}$$

The desired form of the control provides reduction of the projection angle rate $\dot{\Phi}$ to zero. Since the targeted for is

$$\dot{V}\left(\Phi,\dot{\Phi}\right) \simeq -\mathrm{sgn}(g_m(\Phi))g_m(\Phi)h\left(\alpha\dot{\Phi}\right)\dot{\Phi} \tag{17}$$

which expands to the $f(\phi)$ definition in Eq. (12) to the β-modified control expression in Eq. (18).

$$f(\phi_1) = -\frac{\beta}{\sin(\Phi)} - \mathrm{sgn}(g_m(\Phi))h\left(\alpha\dot{\Phi}\right) \tag{18}$$

The leading term in Eq. (18) represents the nominal potential prescribed for electrostatic pushing and pulling. Therefore the β feed-forward gain is defined as

$$\beta = -f(\phi_{\mathrm{nom}})\sin(\Phi) \tag{19}$$

Substituting the resulting new potential of Eq. (18) with the above defined β into the expression in Eq. (16) provides the final form for the Lyapunov derivative.

$$\dot{V}\left(\Phi,\dot{\Phi}\right) = \left[-\beta - \mathrm{sgn}(g_m(\Phi))h\left(\alpha\dot{\Phi}\right)\sin(\Phi) + \beta\right]g_m(\Phi)\dot{\Phi} \tag{20a}$$

$$= -\mathrm{sgn}(g_m(\Phi))g_m(\Phi)\sin(\Phi)h\left(\alpha\dot{\Phi}\right)\dot{\Phi} \tag{20b}$$

which is shown to be negative semi-definite by Reference Bennett et al. (2015) around $\Phi = 0$ and provides asymptotic stability with additional invariant set arguments. Given any nominal pushing or pulling electrostatic potential command β, the control provides asymptotic convergence to a null projection angle rate. Capitalizing on the cancellation of the commanded nominal potential in the stability proof, the nominal equilibrium projection angles from the analysis in Reference Schaub and Stevenson (2012) still apply. Commanding an attractive nominal potential, the cylinder rests at a projection angle of zero. Commanding a repulsive nominal potential rests the cylinder at a projection angle of 90°. However, given that the projection angle describes a 3-dimensional attitude the interpretation of the equilibrium angle is different than previous studies. A projection angle of zero, that of the nominal tugging case, is unambiguous and refers to a perfect alignment between the slender axis of the cylinder and the relative position vector. A projection angle of $\Phi = 90^\circ$ provides an infinite set of attitudes as the projection angle only defines an admissible plane for the slender axis to reside within. Therefore, any combination of body attitudes and angular rates that restricts the slender axis to the plane for all time is admissible as an equilibrium state with nominal repulsive force. The equilibrium surfaces for the nominal tugging and pushing cases are shown in Fig. 4. As it can be seen in Fig. 4, the servicer is thrusting to maintain the fixed relative separation. This 3-dimensional definition of the projection angle fully encapsulates previous results and is applicable to a more general tumble of a debris cylinder.

4. On orbit electrostatic detumble with zero nominal potential

Of further interest is the augmented control law detumble performance while the servicer and debris are in orbit. Prior analysis has only considered the detumble performance in deep space where the relative position vector remains inertially fixed by servicer thrusting (Schaub and Stevenson, 2012; Bennett et al., 2015). The following demonstrates the orbit-independent momentum decrease control law proposed above and discusses final attitudes of the servicer-debris system. The momentum decrease discussion is independent of orbit type. The numerical simulation applies the derived concepts to a lead-follower GEO circular orbit. To stably remove angular momentum from the on orbit debris object, the following Lyapunov function provides conditions on the implemented controller.

$$V = \frac{1}{2}\boldsymbol{\omega}^T I \boldsymbol{\omega} \tag{21}$$

and derivative

$$\dot{V} = \boldsymbol{\omega}^T \boldsymbol{L} \tag{22}$$

where the electrostatic torque is always about the $\hat{\boldsymbol{e}}_L$ vector such that

$$\dot{V} = -L(\boldsymbol{\omega} \cdot \hat{\boldsymbol{e}}_L) \tag{23}$$

Observing Eq. (23) the control design emerges in the prescription of the torque magnitude L. Therefore, for an implemented control to monotonically reduce the angular velocity and thereby the angular momentum, the sign of L is selected such that Eq. (23) is always negative semi-definite. The proposed controller in Eq (12) satisfies this sign requirement and therefore monotonically reduces the angular velocity.

4.1. Investigation of detumble steady-state behavior

Confidence in a stable decrease in angular momentum enables further study into the magnitude of angular momentum dumping. The angular momentum vector components can be expressed along the $\mathcal{E}$-frame and relative position vector with the decomposition graphically represented in Fig. 5. Recall that angular momentum aligned with the relative position vector $H_{\|r}$ cannot be removed in the instantaneous configuration. Using Fig. 5(b) and assuming the relative position vector is fixed inertially, a nonzero $H_{\|r}$ may exist producing a body cone where $\hat{\boldsymbol{b}}_1$

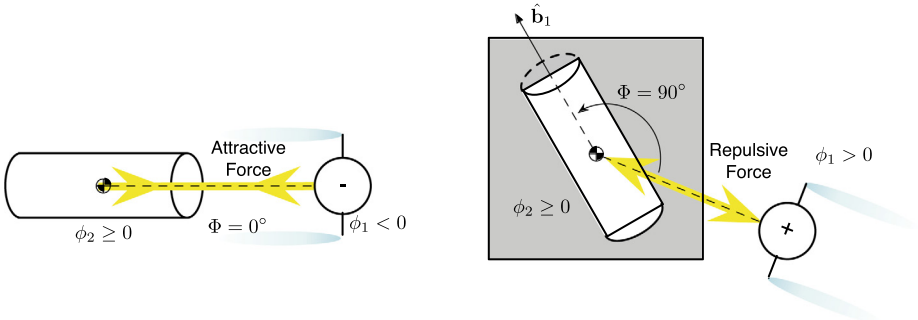

(a) Nominal Tugging (b) Nominal Pushing

Fig. 4. Equilibrium attitudes for nominal tugging and pushing potentials in deep space.

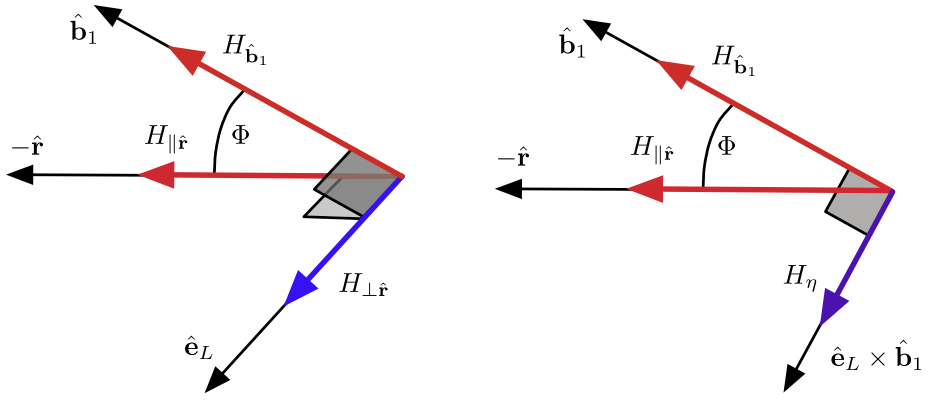

(a) 3D momentum vector components

(b) Planar momentum vector components

Fig. 5. Component breakdown of momentum. Colored to represent the ability for detumble influence. (For interpretation of the references to colour in this figure legend, the reader is referred to the web version of this article.)

sweeps around $\hat{\boldsymbol{r}}$ requiring η to also be nonzero. In such a case, the angular momentum would not be reduced to zero, with a body cone determined by the relative magnitudes of ω_1 and η (Bennett et al., 2015).

Alternatively, if the relative position vector $\hat{\boldsymbol{r}}$ changes inertially, then the momentum decompositions shown in Fig. 5 present an instantaneous snapshot. The magnitude of $H_{\|r}$ is therefore subject to the dynamics of $\hat{\boldsymbol{r}}$ suggesting that reconfiguration may remove greater angular momentum. Recall that the electrostatic torque is only produced around the $\hat{\boldsymbol{e}}_L$ vector defined by Eq. (4). The detumble control produces no torque when the angular momentum derivative and the torque axis are aligned, that is:

$$\boldsymbol{L} = 0 \quad \text{IF} \quad \dot{\boldsymbol{H}} \cdot \hat{\boldsymbol{e}}_L = 0 \tag{24}$$

Study of the cases where the torque does go to zero for all time reveals the steady state behavior of the detumble control. The classical Euler rotational equations are defined for an axi-symmetric body.

$$\dot{\boldsymbol{H}} = \begin{bmatrix} I_a\dot{\omega}_1 \\ I_t\dot{\omega}_2 + (I_a - I_t)\omega_1\omega_3 \\ I_t\dot{\omega}_3 + (I_t - I_a)\omega_1\omega_2 \end{bmatrix} \tag{25}$$

Taking the dot product of Eq. (25) with $\hat{\boldsymbol{e}}_L$ to find where the torque is zero, with η defined in Eq. (7), the null torque definition is obtained.

$$0 = I_t\left[\dot{\omega}_2\left(\hat{\boldsymbol{r}}\cdot\hat{\boldsymbol{b}}_3\right) - \dot{\omega}_3\left(\hat{\boldsymbol{r}}\cdot\hat{\boldsymbol{b}}_2\right)\right] + (I_a - I_t)\omega_1\eta \tag{26}$$

A steady state η can be found if Eq. (26) remains true for all remaining time. The steady state η is therefore:

$$\eta_{ss} = \frac{-I_t}{\omega_1(I_a - I_t)}\left[\dot{\omega}_2\left(\hat{\boldsymbol{r}}\cdot\hat{\boldsymbol{b}}_3\right) - \dot{\omega}_3\left(\hat{\boldsymbol{r}}\cdot\hat{\boldsymbol{b}}_2\right)\right] \tag{27}$$

The leading coefficient of Eq. (27) is constant for the axi-symmetric body. Therefore, the bracketed term of Eq. (27) must remain constant at steady state thereby imposing restrictions on the final momentum of the system. Additional insight is gained through study of the modified projection angle rate equation derived from the time derivative of Eq. (5) with a non-stationary inertial relative position

$$\dot{\Phi}\sin(\Phi) = \omega_3\left(\hat{\boldsymbol{r}}\cdot\hat{\boldsymbol{b}}_2\right) - \omega_2\left(\hat{\boldsymbol{r}}\cdot\hat{\boldsymbol{b}}_3\right) + \left(\hat{\boldsymbol{b}}_1\cdot\dot{\hat{\boldsymbol{r}}}\right) \tag{28}$$

When the controller provides no additional torque for the remainder of time, the projection angle rate must be zero. Therefore, the right hand side of Eq. (28) must be zero. Suppose the controller is successful at removing all the transverse angular velocity when $\hat{\boldsymbol{r}}$ is non-stationary. With the exception of some particular cases, the dot product between the slender axis and the relative position rate must be zero dictating a final projection angle of 90° for all remaining time. A particular degenerate case is where the rotation about the slender axis, ω_1 , assumes the following value for a circular orbit of mean motion, n

$$\omega_1 = \frac{2nI_t}{I_a - 2I_t} \tag{29}$$

Should ω_1 assume the special case value, the cylinder will tumble at a rate that precisely evolves as the orbit does inhibiting further detumble. This suggests that there may be additional cases that do not significantly detumble the target. However, all these cases obey Eq. (28). It can be imagined for rigid body tumble that particular tumble rates would counteract the orbital motion such that the target would remain at a constant projection angle. However, these tumble rates must be at or near the order of the orbit mean motion for the stability and performance control arguments not to be valid. As this study considers a Geosynchronous circular orbit, the detumble to angular rates to the order of the mean motion accomplishes the primary objective of this methodology. As previously stated, mechanical and other capture techniques may be utilized when the tumble rates are of the order of the mean motion.

4.2. Detumble simulation in orbital environment

Three numerical simulations are performed to validate the on-orbit detumbling performance of the deep space control formulation. The first simulation presents the deep space case where gravitational effects are neglected. The second simulation presents the on-oirbit detumble with same initial relative position and tumble conditions as the deep space case and the tugging/pushing control is nominally off. The third simulation introduces a 10 kV tugging control into the on-orbit case. The servicer spacecraft employs closed-loop thrusting controller to maintain a 12.5 meter separation from the target tumbling cylinder. The numerical simulation includes the 6-DOF motion of the debris and 3-DOF translational motion of the servicer sphere. A 4th order Runge-Kutta integration is employed with a time step of 0.01 s. The servicer vehicle potential is controlled via Eq. (12), while the electrostatic force is evaluated using the full MSM model in Eqs. 2,3a,3b. This deep space detumble shown in Fig. 6 re-creates a case from Reference Bennett et al. (2015). The cylinder is generally tumbling with a combined angular velocity of $2^\circ/\text{sec}$. The angular momentum and target cylinder angular velocities are presented in Fig. 6.

The steady-state angular velocities in the presented deep space case are a degenerate case of Eq. (27). The deep space case has a fixed inertial $\hat{\boldsymbol{r}}$ which provides an opportunity for the final coning motion of the debris object to satisfy the bracketed term in Eq. (27) with nonzero transverse angular velocities. Further, with the inertially fixed $\hat{\boldsymbol{r}}$ the $H_{\|r}$ magnitude remains unaffected. Fig. 7(c) shows the inertial $\boldsymbol{H}_Y$ component unchanged where the other two components are driven to zero. The combination of a coning angle and the unchanged parallel angular momentum component produces $\eta_{ss} \neq 0$ and an incomplete angular momentum reduction. Recall in Fig. 2 that a change in relative position, made possible by the natural relative motion while on orbit, could greatly benefit the detumble efficacy. Consider the same initial tumbling conditions presented above with the servicer now leading the debris object in a circular GEO orbit. Given a lead-follower relative orbit, the inertial relative position vector is no longer constant. The resulting detumbling is presented in left column of Fig. 7.

Inspection of the on-orbit cases in Fig. 7(a) and (b) demonstrates the convergence of the ω_2 and ω_3 terms with similar detumble time to the deep space case. The relative motion introduces greater momentum observability by the servicer leading to more effective momentum removal. As expected, the body frame angular velocities for the on orbit cases are reduced to nearly zero while the slender axis ω_1 remains unaffected.

The inertial angular momentum time history in Fig. 7(c) and (d) provide additional support for a more complete debris detumble. Comparison to Fig. 6 reveals that all three inertial momentum vectors are influence when a non-stationary $\hat{\boldsymbol{r}}$ is introduced. The influence of the relative motion is most clear in the nominal on-orbit case, Fig. 7 (c). The final state of the momentum is clearly non-zero despite the dramatic reduction in the angular velocities. The non-zero momentum is a result of neglecting the change in relative position in the development of the detumble controller. As derived, the total energy of the system is monotonically decreasing and the cylinder is moving towards an alignment of the slender axis with the orbit normal for the entire nominal on-orbit case.

As shown in Fig. 7(d), the inclusion of the non-zero tugging introduces additional oscillations in the final momentum states. Recall that the nominal on-orbit detumble case tends towards alignment of the slender axis and the orbit normal. However, the tugging and pushing perturb the cylinder away from these states towards the equilibria shown in Fig. 4. The tugging case demonstrated in Fig. 7 (d) shows that the 10 kV tugging is insufficient to overcome the on-orbit motion and thus injects and removes trace momentum. This is in part due to the magnitude of the force generated by the electrostatic interaction and in part due to the relative geometry between the servicer and the target. Should the magnitude of the electrostatic potential increase then the servicer may be able to tug or push into

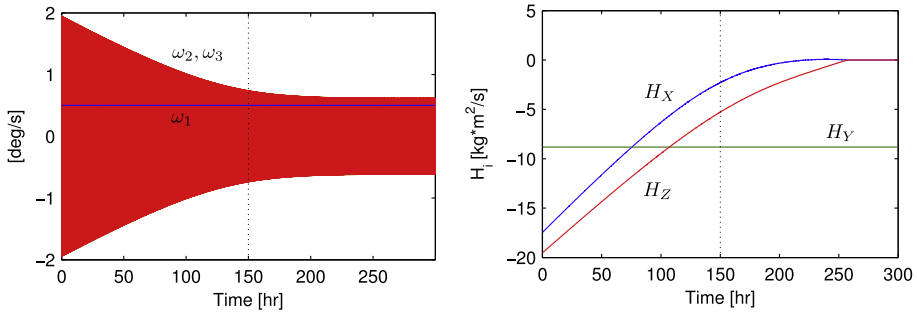

(a) Angular Velocities, Deep Space

(b) Momentum Components H_i in servicer frame

Fig. 6. Angular momentum and velocities with deep space initial conditions: $\omega = [0.5, -1.374, 1.374], \Phi_0 = 30^\circ$ comparing both deep space (left column) and on orbit (right column).

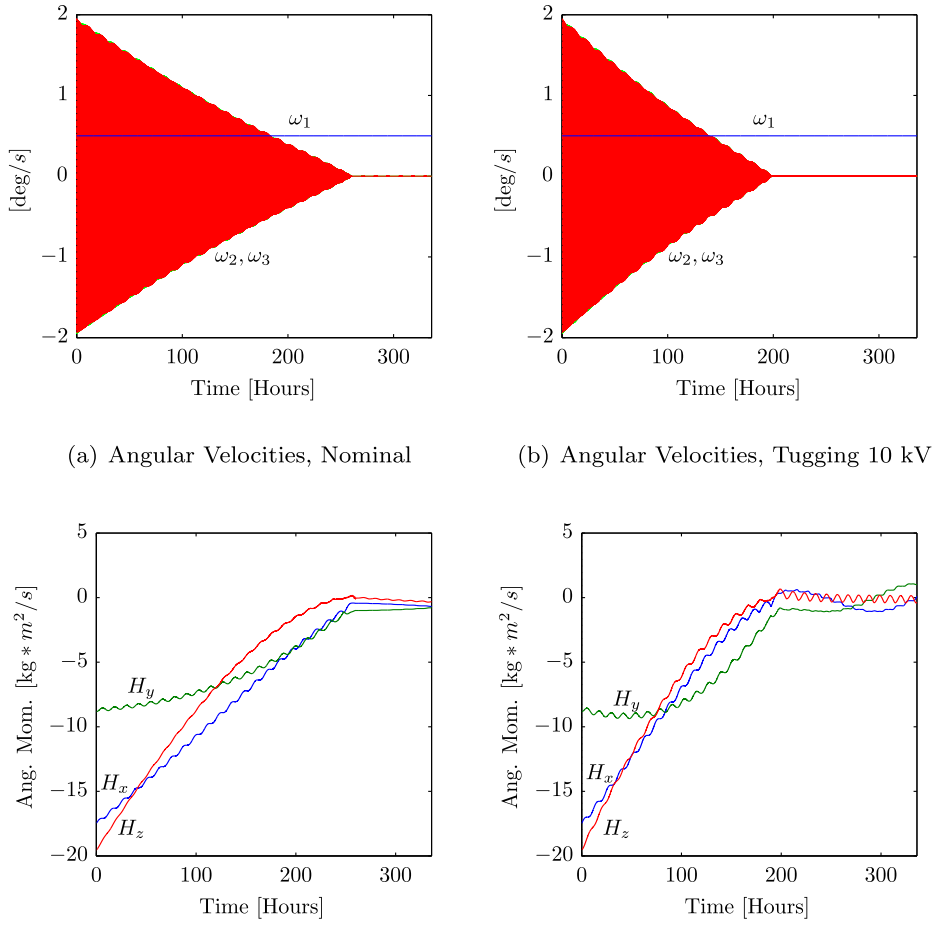

(a) Angular Velocities, Nominal

(b) Angular Velocities, Tugging 10 kV

(c) Nominal momentum, inertial H_i

(d) Tugging momentum, inertial H_i

Fig. 7. Angular momentum and velocities with initial conditions: $\omega = [0.5, -1.374, 1.374], \Phi_0 = 30^\circ$ comparing both nominal (left column) and tugging (right column).

the deep space equilibria states. The control of both on-orbit cases more clearly demonstrate the performance differences between the nominal and tugging control approaches.

Visible at the tail end of the control potential in Fig. 8(a) is a zero-centered periodic control with decreasing magnitude. The inclusion of tugging provides a bias in the control range with a periodic and non-decreasing magnitude control tail in Fig. 8(b). The periodic commanded potential indicates that the implemented control can provide additional momentum dumping after the primary phase. The projection angle history in Fig. 8(c) and Eq. (28) provide sufficient understanding of the supplementary momentum dumping. Inspection of Fig. 8(c) shows a mean oscillation that corresponds directly to the GEO orbit period. The oscillation about this mean is reduced to near zero followed by further reduction of the mean magnitude. This reduction character is dictated by the dominant terms in Eq. (28). During the primary detumble phase, the dominant terms are the body fixed angular velocities which dwarf the $\dot{\hat{\boldsymbol{r}}}$ introduced by a GEO lead-follower relative orbit. Once the angular velocities are sufficiently reduced, the orbit motion contribution becomes dominant and the projection angle begins to collapse towards a steady-state angle. In the deep space case presented in Fig. 4 the angle between the angular momentum and the relative position vector moved towards either 0° or 180°. In the on orbit case, the angular momentum vector appears to oscillate and then collapse towards an angle of 90°. This is supported by Eq. (28) where if the orbital motion remains the dominant term then the $\hat{\boldsymbol{b}}_1$ spin axis must be perpendicular to $\dot{\hat{\boldsymbol{r}}}$ at all future times. Since in a lead-follower relative orbit $\dot{\hat{\boldsymbol{r}}}$ sweeps a plane, then $\hat{\boldsymbol{b}}_1$ must reside perpendicular to the plane. If $\hat{\boldsymbol{b}}_1$ is perpendicular to the plane, which coincides with the orbit plane, then the final projection angle is $\Phi_{ss} = 90^\circ$. Such a projection angle does not appear to violate Eq. (27) and is therefore an admissible final state for the on orbit simulation. The tugging case does not demonstrate the collapse to a projection angle of 90° further supporting the momentum characteristics shown in Fig. 7(d).

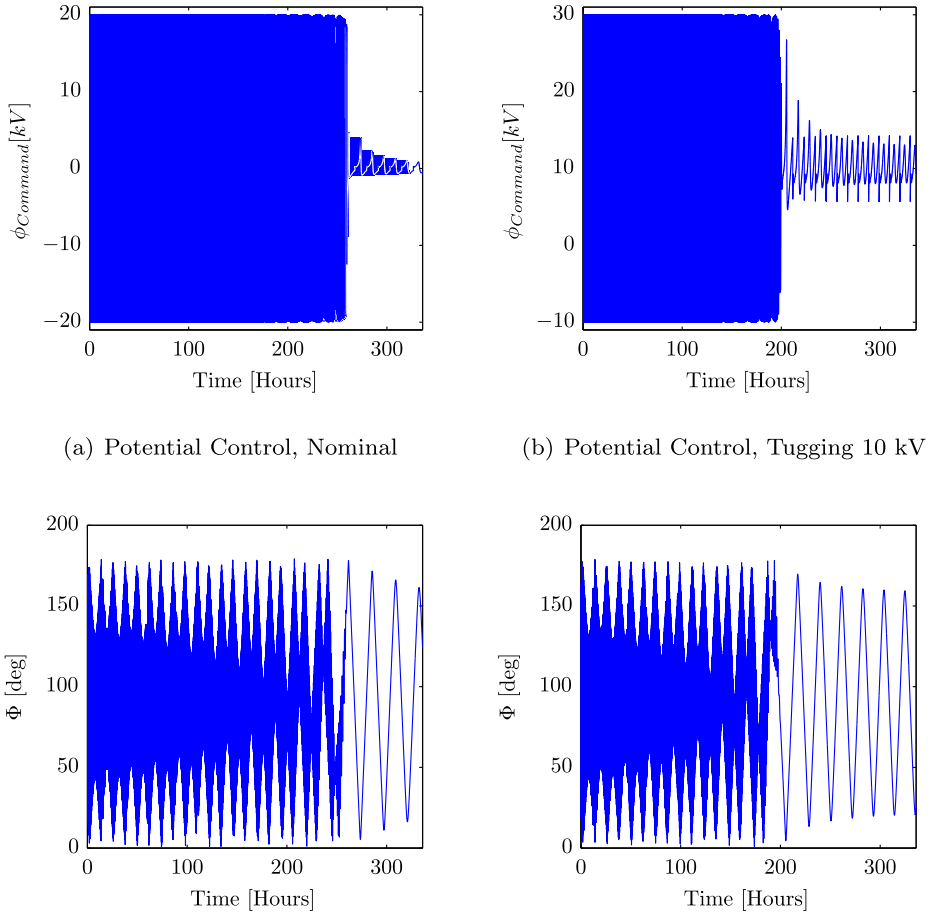

(a) Potential Control, Nominal

(b) Potential Control, Tugging 10 kV

(c) Projection Angle, Nominal

(d) Projection Angle, Tugging 10 kV

Fig. 8. Commanded potential and resulting projection angle with initial conditions: $\omega = [0.5, -1.374, 1.374], \Phi_0 = 30^\circ$ comparing both nominal (left column) and tugging (right column).

5. Conclusions

This study expands a deep space control approach to a 3-dimensional detumble control with simultaneous on-orbit tugging applications. The equilibrium states are derived for nominal, tugging, and pushing conditions. The deep space projection angle dynamics and Lyapunov proof make the projection angle approach zero for nominal tugging and 90° for nominal pushing. The use of the 3-dimensional projection angle allows a full encapsulation of the simplified 1-dimensional rotation case as well as more complex on-orbit configurations. This has the major benefit that the simpler sensing requirements of the deep space based control solution can be applied to the GEO orbiting regime.

The lead-follower GEO simulations demonstrate that the inclusion of simple on orbit relative motion provides increased detumble performance. The addition of a non-stationary inertial relative position vector provides sufficient momentum observability to effectively remove nearly all the non-slender axis momentum. The result is a near-zero final tumble rate that is well within the operational tumble requirements of mechanical docking systems.

Acknowledgments

The authors would like to thank the NASA Space Technology Research Fellowship (NSTRF) program, Grant No. NNX14AL62H, for support of this research.

References

Albuja, A.A., Scheeres, D.J., McMahon, J.W., 2015. Evolution of angular velocity for defunct satellites as a result of YORP: an initial study. Adv. Space Res. 56 (July), 237–251. https://doi.org/10.1016/j.asr.2015.04.013.

Anderson P.V., Schaub, H., 2015. Methodology for characterizing high-risk orbital debris in the geosynchronous orbit regime. In: AAS/AIAA space flight mechanics meeting, Williamsburg, VA, Jan. 11–15 2015. Paper AAS 15-204.

Bennett, T., Schaub, H., 2015. Touchless electrostatic three-dimensional detumbling of large axi-symmetric debris. J. Astronaut. Sci.

Bennett T., Schaub, H., 2016. Capitalizing on relative motion in electrostatic detumbling of axi-symmetric geo objects. In: 6th International Conference on Astrodynamics Tools and Techniques (ICATT), Darmstadt, Germany, March 14–17, 2016.

Bennett, T., Stevenson, D., Hogan, E., McManus, L., Schaub, H., 2015. Prospects and challenges of touchless debris despinning using electrostatics. Adv. Space Res. 56 (Aug), 557–568. https://doi.org/10.1016/j.asr.2015.03.037.

Berryman, J., Schaub, H., 2007. Analytical charge analysis for 2- and 3-craft coulomb formations. AIAA J. Guid. Control Dyn. 30 (Nov.–Dec), 1701–1710.

Bombardelli, C., Pelaez, J., 2011. Ion beam shepherd for contactless space debris removal. AIAA J. Guid. Control Dyn. 34 (May–June), 916–920. https://doi.org/10.2514/1.51832.

Bombardelli, C., Urrutxua, H., Merino, M., Ahedo, E., Pelaez, J., Olympio, J., 2011. Dynamics of ion-beam propelled space debris. In: International Symposium on Space Flight Dynamics, Sao Jose dos Campos, Brasil, Feb. 28 – March 4, 2011.

Caubet, A., Biggs, J.D., 2014. Design of an attitude stabilization electromagnetic module for detumbling uncooperative targets. In: Aerospace Conference, 2014 IEEE, Big Sky, MT, March 1–8.

Chrystal, P., McKnight, D., Meredith, P.L., Schmidt, J., Fok, M., Wetton, C., 2011. Space Debris: On Collision Course for Insurers?, tech. rep., Swiss Reinsurance Company Ltd, Zürich, Switzerland.

Couzin, P., Teti, F., Rembala, R., 2012. Active removal of large debris: Rendez-vous and robotic capture issues. In: 2nd European Workshop on Active Debris Removal, Paris, France, 2012. Paper #7.5.

Couzin, P., Teti, F., Rembala, R., 2013. Active removal of large debris: system approach of deorbiting concepts and technological issues. In: 6th European Conference on Space Debris, Darmstadt, Germany, April 22–25 2013. Paper No. 6a.P-17.

Cover, J.H., Knauer, W., Maurer, H.A., 1966. Lightweight Reflecting Structures Utilizing Electrostatic Inflation, US Patent 3,546,706, October 1966.

Gómez, N.O., Walker, S.J., 2015. Eddy currents applied to de-tumbling of space debris: analysis and validation of approximate proposed methods. Acta Astronaut. 114 (Sept. - Oct.), 34–53. https://doi.org/10.1016/j.actaastro.2015.04.012.

Gómez, N.O., Walker, S.J., 2016. Guidance, navigation, and control for the eddy brake method. J. Guid. Control Dyn. https://doi.org/10.2514/1.G002081.

Hogan E., Schaub, H., 2012. Space debris reorbiting using electrostatic actuation. In: AAS Guidance and Control Conference, Breckenridge, CO, Feb. 3–8 2012. Paper AAS 12–016.

Hogan, E., Schaub, H., 2013. Relative motion control for two-spacecraft electrostatic orbit corrections. AIAA J. Guid. Control Dyn. 36 (Jan. – Feb), 240–249.

Jasper, L.E.Z., Schaub, H., 2014. Tethered towing using open-loop input-shaping and discrete thrust levels. Acta Astronaut. 105, 373–384, De. https://doi.org/10.1016/j.actaastro.2014.10.001.

Karavaev, Y.S., Kopyatkevich, R.M., Mishina, M.N., Mishin, G.S., Papushev, P.G., Shaburov, P.N., 2004. The dynamic properties of rotation and optical characteristics of space debris at geostationary orbit. Adv. Astronaut. Sci. 119, 1457–1466, Paper No. AAS-04-192.

King, L.B., Parker, G.G., Deshmukh, S., Chong, J.-H., 2002. Spacecraft Formation-Flying using Inter-Vehicle Coulomb Forces. tech. rep., NASA/NIAC, January 2002. <http://www.niac.usra.edu>.

Kitamura, S., Hayakawa, Y., Nitta, K., Kawamoto, S., Ohkawa, Y., 2012. A Reorbiter for large geo debris objects using ion beam irradiation. In: 63rd International Astronautical Congress, Naples, Italy, 2012. Paper No. IAC-12-A6.7.10.

Murdoch, N., Izzo, D., Bombardelli, C., Carnelli, I., Hilgers, A., Rodgers, D., 2008a. Electrostatic tractor for near Earth object deflection. In: 59th International Astronautical Congress, Glasgow Scotland, 2008. Paper IAC-08-A3.I.5.

Murdoch, N., Izzo, D., Bombardelli, C., Carnelli, I., Hilgers, A., Rodgers, D., 2008b. The electrostatic tractor for asteroid deflection. In: 58th International Astronautical Congress, 2008. Paper IAC-08-A3.I.5.

Ogilvie, A., Allport, J., Hannah, M., Lymer, J., 2008. Autonomous satellite servicing using the orbital express demonstration manipulator system. In: Proc. of the 9th International Symposium on Artificial Intelligence, Robotics and Automation in Space (i-SAIRAS'08), Hollywood, CA, February 26-29 2008, pp. 25–29.

Peck, M.A., 2005. Prospects and challenges for Lorentz-augmented orbits. In: AIAA Guidance, Navigation and Control Conference, San Francisco, CA, August 15–18 2005. Paper No. AIAA 2005-5995.

Peck, M.A., Streetman, B., Saaj, C.M., Lappas, V., 2007. Spacecraft formation flying using lorentz forces. J. Br. Interplanet. Soc. 60 (July), 263–267.

Praly, N., Hillion, M., Bonnal, C., Laurent-Varin, J., Petit, N., 2012. Study on the eddy current damping of the spin dynamics of space debris from the Ariane launcher upper stages. Acta Astronaut. 76, 145–153.

Reed, J., Busquets, J., White, C., 2012. Grappling system for capturing heavy space debris. In: 2nd European Workshop on Active Debris Removal, Paris, France. Paper 4.2.

Schaub, H., Stevenson, D., 2012. Prospects of relative attitude control using coulomb actuation. In: Jer-Nan Juang Astrodynamics Symposium, College Station, TX, June 25–26 2012. Paper AAS 12–607.

Seubert, C.R., Panosian, S., Schaub, H., 2012. Analysis of a tethered coulomb structure applied to close proximity situational awareness. AIAA J. Spacecraft Rockets 49 (Nov. – Dec), 1183–1193.

Sliško, J., Brito-Orta, R.A., 1998. On approximate formulas for the electrostatic force between two conducting spheres. Am. J. Phys. 66 (4), 352–355.

Smythe, W.R., 1968. Static and Dynamic Electricity, third ed. McGraw–Hill.

Starke, J., Bischof, B., Foth, W.H., Guenther, H.J., 2009. ROGER, a Potential Orbital Space Debris Removal System. In: NASA/DARPA International Conference on Orbital Debris Removal, Chantilly VA, December 8–10 2009.

Stevenson, D., Schaub, H., 2013. Multi-sphere method for modeling electrostatic forces and torques. Adv. Space Res. 51 (Jan), 10–20. https://doi.org/10.1016/j.asr.2012.08.014.

Stiles, L.A., Schaub, H., Maute, K.K., Moorer, D.F., 2013. Electrostatically inflated gossamer space structure voltage requirements due to orbital perturbations. Acta Astronaut. 84 (Mar.–Apr), 109–121. https://doi.org/10.1016/j.actaastro.2012.11.007.

Streetman, B., Peck, M.A., 2007. New synchronous orbits using the geomagentic lorentz force. AIAA J. Guid. Control Dyn. 30 (Nov.–Dec), 1677–1690.

Vatrisano, M., Thiry, N., Vasile, M., 2015. Detumbling large space debris via laser ablation. In: IEEE Aerospace Conference, Big Sky, Montana, March 7–14, 2015.

Vetrisano, M., Colombo, C., Vasile, M., 2016. Asteroid rotation and orbit control via laser ablation. Adv. Space Res. 57 (8), 1762–1782. https://doi.org/10.1016/j.asr.2015.06.035.

Wang, S., Schaub, H., 2011. Nonlinear charge control for a collinear fixed shape three-craft equilibrium. AIAA J. Guid. Control Dyn. 34 (Mar.–Apr), 359–366. https://doi.org/10.2514/1.52117.

Xu, W., Liang, B., Li, B., Xu, Y., 2011. A universal on-orbit servicing system used in the geostationary orbit. Adv. Space Res. 48 (1), 95–119. https://doi.org/10.1016/j.asr.2011.02.012.

Yamakawa, H., Bando, M., Yano, K., Tsujii, S., 2010. Spacecraft relative dynamics under the influence of geomagnetic lorentz force. In: AIAA Guidance, Navigation and Control Conference, Toronto, Canada, Aug. 2–5 2010. Paper No. AIAA 2010-8128.

Yamamoto U., Yamakawa, H., 2008. Two-craft coulomb-force formation dynamics and stability analysis with debye length characteristics. In: AIAA/AAS Astrodynamics Specialist Conference and Exhibit, Honolulu, Hawaii, Aug. 18–21 2008. Paper No. AIAA 2008-7361.